Line Shapes in Infrared Absorption by Solids and by Atomic or Molecular Species Embedded in Solids

Miguel Lagos,*,† Felipe A. Asenjo,‡ Roberto Hauyón,‡ Denisse Pastén,‡ and Pablo S. Moya‡

Departamento de Ciencias Aplicadas, Facultad de Ingeniería, Universidad de Talca, Campus Los Niches, Curicó, Chile, and Departamento de Física, Facultad de Ciencias, Universidad de Chile, Casilla 653, Santiago, Chile

Received: April 17, 2010; Revised Manuscript Received: June 1, 2010

When the target is in the solid state, most infrared spectral features are manifestly asymmetric; hence, a line shape function well-grounded in theory is necessary to ascertain the net energy taken by the associated electronic transition. The main sources for spectral line broadening, asymmetry, and shift, no matter the transferred energy, are multiphonon events involving the acoustic vibrational modes. A simple closed-form mathematical expression for the phonon-broadened lineshapes, shown to be valid at low temperatures, and linewidths on the order of the Debye energy of the solid or smaller, giving remarkable agreement with experiment is studied in connection with its utility for analyzing infrared spectral features.

Introduction

Despite the capital role infrared spectroscopy has played in the study of molecular structure and dynamical properties, the recognition of chemical species and determination of their relative presence in heterogeneous environments and a number of other very fundamental applications, there is still an unsolved technical question. If the target is in a condensed thermodynamic phase, the shapes of the spectral features and the position of the maxima are modified in a temperature-dependent manner. When the temperature-dependent width of an absorbance peak is comparable to or smaller than the Debye energy of the solid, the absorption line generally exhibits noticeable asymmetry. In most cases, the peak side corresponding to lower photon energies is steeper than the other side, but the opposite situation is possible, as well, albeit seldom. The interpretation of the inverse asymmetry is quite interesting because it seems to contradict the entropy principle.

Identifying the optical frequency associated to maximum absorption or emission with the peak position and interpreting it as the energy of the corresponding electronic transition may be not a bad practice because most asymmetrical features are relatively narrow, but anyway, it introduces an error. In general, the maximum of asymmetric bands shifts with temperature. This error is particularly significant in the far-infrared spectral region, where the frequencies are small enough to be comparable to the peak widths and may be not negligible also in the near-infrared. It is shown below that, as a general rule, the net energy taken by an electronic transition is never coincident with the maximum of the corresponding spectral feature. Both photon capture and emission processes produce a sudden nonadiabatic disturbance of the condensed medium. Statistically, they involve entropy production and, hence, dissipate net energy into the thermal bath at the expenses of the radiation field. Depending on the strength of the coupling of the disturbed electronic bond with the elementary excitations of the condensed environment, this effect may manifest in the absorption (emission) spectra as either approximately symmetric spectral features displaced toward higher (lower) energies or the production of asymmetric spectral maxima with a steeper low (high) energy side. Color centers, usually evidencing large Stokes shifts, pertain to the former case, and the excitation of vibronic modes and most infrared features are in the latter.[1−4]

A main part of the harmonic forces between the crystal ions comes from the adiabatic shifts played by the energy levels of the electronic bonds when the ionic relative positions change. By virtue of the adiabatic approximation, the electronic degrees of freedom disappear and become implicit in the force constants governing the ionic motions. Notwithstanding, because of the large mass ratio between ionic cores and electrons, the electromagnetic radiation field interacts mostly with the electronic bonds. This way, any interaction of the electromagnetic field with the nuclear motions is via a nonadiabatic alteration of the local force constant of the solid. From this viewpoint, localized vibronic modes can be dealt with as electronic degrees of freedom when focusing their interaction with electromagnetic radiation.

Therefore, determining the net excitation energy of an electronic bond or vibronic mode from an asymmetrical spectral feature demands precise knowledge of the concurrent energy transfers taking place in the target. Otherwise, the error bonds will be dictated not by the experimental device but by the incomplete knowledge of how it works. Consider, for instance, the absorption peak observed by Takeno and Sievers for substitutional Ag^+ in KI.[5] For temperature $T = 10.4$ K, the maximum is at a wavenumber $k = 18.1$ cm^{-1}, and the full width at half-maximum (fwhm) is $2\Gamma = 1.6$ cm^{-1}; that is, almost 10% of the peak position. As the temperature is reduced to $T = 7.4$ K, the maximum shifts to $k = 17.2$ cm^{-1}, and the fwhm changes to $2\Gamma = 1.4$ cm^{-1}. A refined analysis of the experimental data revealed that the real frequency of the electronic transition, which must not depend on temperature, is $k = 17.17$ cm^{-1} in the two spectra.[6]

The example recalled above illustrates the convenience of having an accurate model for the line shape, well founded on the physics of the photon absorption or emission process. Judging by the peak position in the two spectra, the frequency

* To whom correspondence should be addressed: E-mail: mlagos@utalca.cl.
† Universidad de Talca.
‡ Universidad de Chile.

10.1021/jp103459p
Published on Web 06/17/2010

of the local mode of Ag^+ in KI is 17.2 − 18.1 cm^{-1}; however, the line shape study gives a figure as precise as 17.17 cm^{-1}. The dramatic accuracy improvement occurs because the latter result has the precision of barely the experimental setup, whereas the former is affected also by unresolved phenomena taking place in the target.

The literature shows extensive studies on the line shape of the optical spectra, considering a variety of line broadening sources, such as Doppler shifts, molecular collisions, crystal defects, inhomogeneous strains, and many others. The most commonly used distributions for the spectral analysis are the Gauss distribution, accounting for Doppler shifts, and Voigt distribution,[7] which convolutes a Gauss and a Lorentz distribution in an attempt to incorporate collisions and more complex sources of energy dispersion. Both are ineffective for our purposes because they are symmetric. A recent paper put forward an empirical method for imparting asymmetry to these distributions.[8] Although fitting well the experimental data, the procedure gives just a good interpolation formula because it is not based on the physics of the optical transitions.

When the target is in the solid state, the main source for line broadenings are the acoustic crystal modes. Acoustic phonons have no energy threshold and obey Bose−Einstein statistics; hence, any local electronic transition which modifies in any way the equilibrium of the surrounding lattice will excite and de-excite many crystal modes. No matter the magnitude of the energy involved, the process will be a multiphonon event.[6] This is apparent from experiment, since zero-phonon lines, which are expected to have significant intensity in few-phonon processes, are infrequent in the infrared spectra.[9,10] This way, acoustic phonons are always present: widening, shifting, and deforming the spectral features. The good new is that simple closed-form mathematical expressions can be written for the profiles of the electromagnetic absorption and emission bands.[6]

Transitions involving relatively high energies, such as the excitation to a higher-energy atomic or molecular stationary state, of either an impurity center or a main constituent of the crystal couple strongly with the lattice modes and give rise to wide bands of several tenths of an electronvolt in width. They are usually in the visible (color centers) or near-infrared spectral regions. On the other hand, the excitation of local modes of point defects, or internal vibrations of molecular bonds, couple weakly with the lattice and produce narrow asymmetrical bands in the infrared or far-infrared, whose widths are in the range 0.1−10 meV. The shape of these narrow infrared bands is our main concern here. We will show they can be accurately described by a simple line shape function, whose only parameters are the net energy of the electronic transition and an asymmetry coefficient, both temperature-independent, and the temperature-dependent peak width. The theory assumes linear electron−phonon coupling, which is accurate enough for dealing with optical transitions in the infrared.[6] Quadratic coupling is far beyond our needs because it implies substantial modification of the electronic bonds.[11] Anharmonicity is also not considered because we are not occupied here with higher order effects or fine details of spectra. Examining real spectra, line shape asymmetries are neither uncommon nor small when compared with the corresponding line widths. Our main purpose here is to link recently published theoretical achievements,[6] which put strong emphasis on the mathematical derivations, with the needs of experimental spectroscopists to interpret their data.

The General Phonon Widened Line Shape Function

The Line Shape Function. In general, the one-photon spectral feature associated with the transition between the localized electronic states l and l' in an elastic environment is given by the integral expression[6]

$$F_{l'l}(\hbar ck;T) = \int_{-\infty}^{\infty} \mathrm{d}t \exp\left\{ \sum_q |G_{ql'l}|^2 \times \left[-2 \coth\left(\frac{\hbar\omega_q}{2k_B T}\right) \sin^2(\omega_q t/2) + i \sin(\omega_q t) \right] \right\} \frac{\exp[-i(ck - E_{l'l}/\hbar)t]}{2\pi\hbar} \tag{1}$$

which satisfies

$$\int_{-\infty}^{\infty} \mathrm{d}(\hbar ck)\, F_{l'l}(\hbar ck;T) = 1 \tag{2}$$

Here, $E_{l'l}$ is the energy difference between the two electronic states, which will be the discussed in detail in a forthcoming subsection. $\hbar ck$ is the photon energy, c denoting the speed of light, and $k = 2\pi/\lambda$, with λ the wavelength, the wavenumber. Index $q = (\mu, \vec{q})$ stands for the crystal vibrational mode of the branch μ whose wave vector, frequency, and polarization vector are $\vec{q}$, ω_q, and $\hat{e}_q$. The branch index, μ, may also characterize localized modes associated with eventual crystal defects. The coefficients $|G_{ql'l}|^2$ will be defined in the next subsection.

The Physical Bases for the Line Shape Function. Just to make clear the general character of the line shape expression (eq 1) and the assumptions it involves, we briefly review its derivation.[6] The Hamiltonian of the solid, having eventual lattice imperfections, is

$$H_0 = \sum_q \hbar\omega_q a_q^\dagger a_q + \sum_l \varepsilon_l c_l^\dagger c_l + \sum_{ql} g_{ql} c_l^\dagger c_l (a_q - a_{\bar{q}}^\dagger) \tag{3}$$

where a_q is a phonon operator. The fermion operator, $c_l^\dagger$, with $l = (\alpha, \vec{l})$, creates an electron in internal excitation state $\psi_\alpha(\vec{r}\text{-}\vec{l})$ with energy ε_l bound to the site $\vec{l}$. The operator $c_l^\dagger c_l$ accounts for the internal state of the ion, or binding orbital, located at the crystal site $\vec{l}$. The eigenstates of H_0 for which the eigenvalue of $c_l^\dagger c_l$ vanishes for any l effectively reduce the operator, eq 3, to just its first term, which represents a standard harmonic solid. They describe the dynamics of the unperturbed crystal, with all its ions in the ground state. The second and third terms of H_0 account for the possibility of the internal states of the crystal constituents to be excited. Notice that off-diagonal terms of the form

$$H_1 = \sum_{l \neq l'} \sum_q g_{ql'l} c_{l'}^\dagger c_l (a_q - a_{\bar{q}}^\dagger) \qquad (l' \neq l) \tag{4}$$

are not considered in H_0. The terms in $g_{ql'l}$ may contribute to the phonon-assisted hybridization of the electronic states, turning their energy levels into bands of finite width. H_1 is a comparatively small term but may acquire importance at high enough temperatures. Its neglect is usually referred to as the Condon approximation.

The linear electron−phonon coupling coefficients of H_0 have the explicit expression

$$g_{ql} = \sqrt{\frac{\hbar}{2NM_{\vec{l}}\omega_q}}\hat{e}_q \cdot \sum_{\vec{l}'} e^{i\vec{q}\cdot\vec{l}'}\vec{F}_{\alpha(\vec{l}-\vec{l}')} \quad (5)$$

where N is the number of atoms in the sample, $M_{\vec{l}}$ is the mass in site $\vec{l}$, and $\vec{F}_{\alpha(\vec{l}-\vec{l}')}$ is the expectation value of the force exerted on the ion at $\vec{l}$ by the one at $\vec{l}'$, both assumed in internal state α. The coefficients $|G_{ql'l}|^2$ appearing in eq 1 are given by

$$G_{ql'l} = \frac{g_{ql'} - g_{ql}}{\hbar\omega_q} \quad (6)$$

The line shape function, eq 1, follows from calculating the single photon transition probability per unit time of the electromagnetic field, whose free Hamiltonian reads

$$H_2 = \sum_{\nu\vec{k}} \hbar ck \eta^{\dagger}_{\nu\vec{k}}\eta_{\nu\vec{k}} \quad (7)$$

when expressed in terms of the photon operators $\eta_{\nu\vec{k}}$ of wavevector $\vec{k}$ and polarization index ν, coupled with the electronic degrees of freedom of H_0 by the interaction term

$$H_3 = \sqrt{\frac{c}{V}}\sum_{l'l} Q_{l'l\nu\vec{k}} c^{\dagger}_{l'} c_l (\eta_{\nu\vec{k}} - \eta^{\dagger}_{\nu(-\vec{k})}) \quad (8)$$

where $Q_{l'l\nu\vec{k}}$ is an electron−photon coupling coefficient, for any final and thermally weighted initial state of the vibrational modes. No restriction on the number of exchanged phonons in each virtual process is made.

Employing the methods of quantum field theory, the mathematical procedure can be accomplished exact and rigorously, with no additional assumptions,[6] and hence, eq 1 is as general and accurate as is H_0. In particular, no assumption is made on the size of the coefficients $G_{ql'l}$, which determine the bandwidth. Therefore, eq 1 is valid for either wide and narrow bands. An expression similar to eq 1 has been written in the past,[2] but was derived from the less general theory of Huang and Rhys[12] for color centers, based on the semiclassical Franck−Condon principle.[13,14] The semiclassical approach was believed to hold just for wide bands because they are associated with shorter transition times by the uncertainty principle. The recent more rigorous treatment[6] demonstrates that eq 1 can be safely employed to study any optical feature, no matter the width.

The Transition Energy $E_{l'l}$. The eigenvalue spectrum of H_0 is given by[6]

$$E_{l\{n_q\}} = \sum_{\{n_q\}} \hbar\omega_q n_q + \sum_l \left(\varepsilon_l - \sum_q \frac{|g_{ql}|^2}{\hbar\omega_q}\right) m_l \qquad n_q = 0, 1, 2, ..., \quad m_l = 0, 1 \quad (9)$$

where the nonnegative numbers n_q account for the excitation state of the vibrational modes q, and m_l stands for the excitation state of the orbital at $\vec{l}$. The energy, ε_l, is the energy of the electronic orbital $l = (\alpha, \vec{l})$ when the nuclei or ionic cores are all fixed to their corresponding lattice sites, $\{\vec{l}\}$. On the other hand, the crystal lattice, $\{\vec{l}\}$, is defined as the set of the equilibrium positions of the nuclei when all the electronic orbitals are in their ground state. Thus, the promotion of one orbital from its ground state to an excited state, l, conveys a local lattice distortion whose magnitude is governed by the electron−phonon coefficients g_{ql}, which vanish when l represents the ground state. Therefore, we can interpret

$$E_l \equiv \varepsilon_l - \sum_q \frac{|g_{ql}|^2}{\hbar\omega_q} \quad (10)$$

as the energy of an excited electronic orbital at $\vec{l}$ coupled to the rest of the solid by the linear electron−phonon interaction. The first term in the right-hand side of eq 10 represents the excitation energy with no lattice deformation, and the second one is the corresponding lattice relaxation energy.

The energy term, eq 10, does not depend on the vibrational state, $\{n_q\}$, of the solid. It is characterized by only the electronic quantum number l and, hence, can be considered as the net energy of the electronic orbital in the solid environment. However, it depends on the elastic force constants of the solid through the relaxation energy term.

Together with the intensity factor, spectroscopy experiments measure the normalized distribution, $F_{l'l}(\hbar ck; T)$. As shown by eq 1, the transition energy

$$E_{l'l} = E_{l'} - E_l \quad (11)$$

plays the role of a displacement along the $\hbar ck$ axis in a plot of the line function $F_{l'l}$. Hence, the temperature-independent difference eq 11 determines the line position and is usually the main value the spectral feature can retrieve. It is apparent from the previous discussion that the line center, $E_{l'l}$, is in general dependent on the precise nature of the solid environment, and the spectra of a same molecule embedded in different solids should exhibit line shiftings.

The Line Shape Is Always Asymmetric. The photon energy distribution, eq 1, can be split as

$$F_{l'l}(\hbar ck;T) = F^{(e)}_{l'l}(\hbar ck;T) + F^{(o)}_{l'l}(\hbar ck;T) \quad (12)$$

with

$$F^{(e)}_{l'l}(\hbar ck;T) = \int_{-\infty}^{\infty} dt \exp\left[-2\sum_q |G_{ql'l}|^2 \coth\left(\frac{\hbar\omega_q}{2k_BT}\right)\sin^2(\omega_q t/2)\right] \times \cos\left[\sum_q |G_{ql'l}|^2 \sin(\omega_q t)\right] \frac{\cos[(ck - E_{l'l}/\hbar)t]}{2\pi\hbar} \quad (13)$$

an even function of $\hbar ck - E_{l'l}$, and

$$F^{(o)}_{l'l}(\hbar ck;T) = \int_{-\infty}^{\infty} dt \exp\left[-2\sum_q |G_{ql'l}|^2 \coth\left(\frac{\hbar\omega_q}{2k_BT}\right)\sin^2(\omega_q t/2)\right] \times \sin\left[\sum_q |G_{ql'l}|^2 \sin(\omega_q t)\right] \frac{\sin[(ck - E_{l'l}/\hbar)t]}{2\pi\hbar} \quad (14)$$

which is odd in $\hbar ck - E_{l'l}$. Therefore, the component $F^{(e)}_{l'l}(\hbar ck; T)$ of the exchanged electromagnetic energy distribution is symmetric with respect to the electronic excitation energy, $E_{l'l}$, and

function $F_{l'l}^{(0)}(\hbar ck; T)$ is an antisymmetric correction. Because $F_{l'l}^{(0)}$ does not vanish identically, spectral maxima are expected not to be at the exact transition energies $E_{l'l}$.

The adoption of a linear Debye model for the crystal acoustic modes, which are the only contributors for narrow lines because eventual optical and localized branches produce separate peaks,[6] allows one to write eq 1 in a more explict form. Because very low vibrational frequencies prove to contribute the most, the linear dispersion relation is also expected to give good precision. However, we will show next that the integrals in eq 1 can be solved by introducing no specific model, but just three parameters having very clear physical meaning. Notwithstanding, the particularization to a Debye model may be useful to rapidly perceive the general properties of the functions involved, we refer the reader to the previous literature,[6] where an illustrative example is given.

Asymptotic Line Shape for Weak Electron−phonon Coupling

The absolute value of the subintegral function in eq 1 has a maximum at $t = 0$, which will be referred to as the *central maximum* and decays in an oscillating manner to a constant as $|t|$ grows, which gives rise to the zero-phonon line. We will refer to the side oscillating decays as the *tails* of the subintegral function. If the coefficients $|G_{q'l'l}|^2$ are big, the central maximum is narrow and decays rapidly as a Gauss distribution, and the integral converges quickly because the oscillating tails yield little contribution. When the coefficients $|G_{q'l'l}|^2$ are small, the integral exhibits poor convergency, the central maximum has a marginal relative role, and the tails contribute the most to the integral. In the extreme case of $|G_{q'l'l}|^2 = 0$, the line shape function becomes a δ-function.

From examining eqs 5 and 6, one can realize that $G_{q'l'l}$ is proportional to the mean force variations upon the orbital excitation $l \rightarrow l'$. Hence, for weak electron−phonon coupling, what matters is the asymptotic behavior for large values of $|t|$. As was done before,[6] we make

$$\frac{\sin(\omega_q t)}{\omega_q} \approx \pi\delta_1(\omega_q)\frac{t}{|t|} \rightarrow \begin{cases} \pi\delta(\omega_q) & (t \rightarrow \infty) \\ -\pi\delta(\omega_q) & (t \rightarrow -\infty), \end{cases}$$
$$\left[\frac{\sin(\omega_q t/2)}{\omega_q}\right]^2 \approx \frac{\pi}{2}\delta_1(\omega_q)|t| \rightarrow \frac{\pi}{2}\delta(\omega_q)|t| \quad (t \rightarrow \pm\infty) \tag{15}$$

where δ_1 is a finite distribution that approaches a δ-function for large t. Replacing in eq 1 and integrating, one obtains

$$F_{l'l}(\hbar ck;T) = \frac{1}{\pi}\frac{\cos\delta_{l'l}\Gamma_{l'l}(T) + \sin\delta_{l'l}(\hbar ck - E_{l'l})}{(\hbar ck - E_{l'l})^2 + [\Gamma_{l'l}(T)]^2} \tag{16}$$

where

$$\Gamma_{l'l}(T) = \pi\sum_q \hbar\omega_q^2|G_{q'l'l}|^2 \coth\left(\frac{\hbar\omega_q}{2k_B T}\right)\delta_1(\omega_q) \tag{17}$$

is the half width at half-maximum (hwhm) of the distribution and

$$\delta_{l'l} = \pi\sum_q \omega_q|G_{q'l'l}|^2\delta_1(\omega_q) \tag{18}$$

governs the asymmetry.

Notice that we gave all credit to the tails for obtaining eq 16 and neglected the central maximum. However, as $|ck - E_{l'l}/\hbar|$ is increased, the exponential factor in the subintegral function of integral eq 1 will oscillate with increasing speed, and the tails rapidly will average to zero. In such a case, the small contribution of the central maximum will predominate. Hence, the relative accuracy of the asymptotic distribution eq 16 will be lost for large enough values of $|\hbar ck - E_{l'l}|$, where $F_{l'l}(\hbar ck; T)$ is small.

Application to the Analysis of Spectral Features

We turn now to the main purpose of this article, which is to relate recently published achievements,[6] whose emphasis on the mathematical derivations may obscure the reach of the results, with the needs of experimental spectroscopists to interpret their data. The first points are how to make sure that the data is in the proper asymptotic limit and how the limitations of the line shape asymptotic expression eq 16 may come to the fore.

To go right into the matter, consider the spectral peak of solid NH_3 observed by Gerakines et al.[15] at $k = 1/\lambda = 4993$ cm^{-1} and $T = 10$ K (Figure 8 of their paper). The open circles in Figure 1 reproduce the experimental data with the top of the peak normalized to unity; the solid curve represents the fit given by eq 16. Although the peak of the distribution is at $k = 4993$ cm^{-1}, for the energy of the electronic transition, the fit gives $E_{l'l}/(hc) = 4997.5$ cm^{-1}. Although the accuracy of the fit is remarkable, the most stringent test of the theory is coming next.

Examine now eq 16 and notice that, due to the antisymmetric component proportional to sin δ, the higher (lower) photon energy side of $F_{l'l}$ decays as $(\hbar ck - E_{l'l})^{-1}$ when $\delta > 0$ (when $\delta < 0$). The other side of $F_{l'l}$ (the steeper one) has a zero, but we know from a previous discussion that the asymptotic expression eq 16 ceases to be valid for $F_{l'l} \approx 0$. Hence, the zero in the steeper side of $F_{l'l}$ determines a bound for the range of the distribution.

The other bound follows from examining Figure 2, which plots the logarithm of the $(k - E_{l'l}/(hc))^{-1}$ side of the peak represented in Figure 1 (corresponding to lower photon energies because $\delta < 0$) versus $\log|k - E_{l'l}/(hc)|$. (Notice that now, $k = 1/\lambda$ instead of $k = 2\pi/\lambda$, as in the previous sections; we adapt ourselves to the usual notation in spectroscopic studies). The equation for the straight line appearing in Figure 2 is $\log F = -\log|k - E_{l'l}/(hc)| + 1.39$. The coincidence of the experimental points for large values of $|k - E_{l'l}/(hc)|$ with the -1 slope line is impressive. Observe that the $|k - E_{l'l}/(hc)|^{-1}$ decay of the less steep side of the peak is due to the dominance of the odd term of the distribution, responsible for the asymmetry; the other Lorentzian term decays as $|k - E_{l'l}/(hc)|^{-2}$. Because the Fourier transformation is a bijective operation, the accurate fit of the data to the $(k - E_{l'l}/(hc))^{-1}$ law shows that the substitution in eq 15 of the exact functions with their asymptotic expressions is the right analytic condition for the physics of narrow spectral bands.

Finally, notice the three last experimental points at the extreme right in Figure 2, defying the tendency to align along the straight line $\log F = -\log|k - E_{l'l}/(hc)| + 1.39$. They are quite revealing because they mark the other bound for the range in which the asymptotic approximation eq 15 does hold. The plot shown in Figure 2 constitutes a good method for determin-

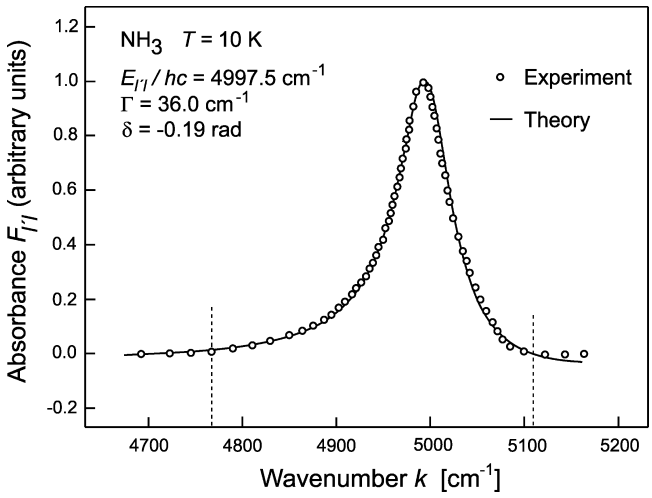

Figure 1. Infrared absorption by solid NH_3 at $T = 10$ K. Open circles represent experimental data of Gerakines et al.,[15] and the solid line depicts eq 16 with the parameters given in the inset. The maximum is at $k = 4993$ cm^{-1} and the energy $E_{l'l}$ of the electronic transition is such that $E_{l'l}/(hc) = 4997.5$ cm^{-1}. The dashed vertical lines mark the bounds within which eq 16 is accurate.

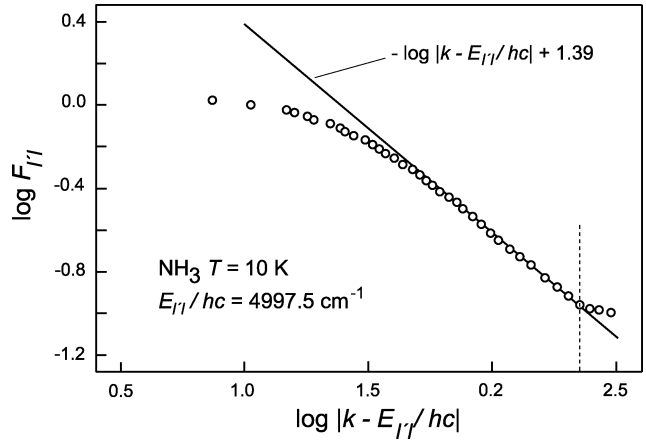

Figure 2. Logarithmic plot of the experimental points of the less abrupt side of the spectral feature shown in Figure 1. The slope of the straight line is -1, as predicted by eq 16. The three points in the extreme right are beyond the bounds within which eq 16 is valid. This kind of plot constitutes a useful tool for determining such bounds.

ing from the experimental data the range in which eq 16 is expected to hold. The best way to proceed is to determine first the bound of the less abrupt side of the peak from the logarithmic graph, as in Figure 2, and then to assign the other bound to the point corresponding to the same value of $F_{l'l}$ in the steeper side. The position of the dotted lines in Figure 1 was chosen this way. The criterion of the zero of $F_{l'l}$ in the steeper side, which was explained before, is too extreme.

Together with linewidths of less than, or on the order of, the Debye energy of the solid, low enough temperatures that keep negligible the contribution of the term H_1 are the basic conditions for the validity of the asymptotic line shape function, eq 16. On the basis of our experience, $T < 20$ K is sufficient in most cases. However, the best procedure is to take data for at least two different temperatures to make sure that the corresponding theoretical fits give the same values for $E_{l'l}$ and $\delta_{l'l}$ (e.g., see Table 3 of Lagos et al.[6]).

Figure 3 shows another example of the application of eq 16 to a solid mixture of water and methane.[16] Notice the much narrower line width and the positive value for δ. In general, eq 16 gives the same good fit to any near,[15,16] and far[5,6] infrared

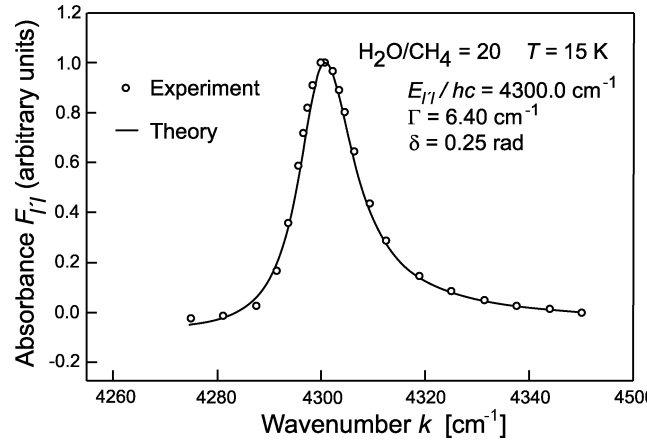

Figure 3. Data of Bernstein et al.[16] on the infrared absorption by a solid mixture of 20 parts of H_2O to one of CH_4. Solid line represents eq 16.

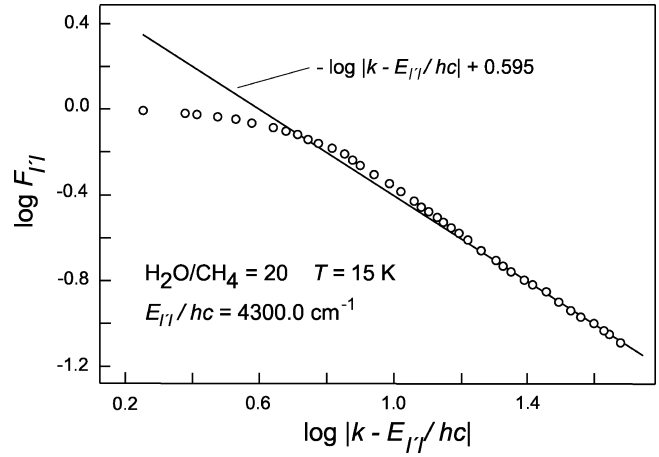

Figure 4. Logarithmic plot of the experimental points of the less steep side of the spectral peak of Figure 3 on the infrared absorption by a solid mixture of 20 parts of H_2O to one of CH_4. The slope of the straight line is -1.

spectral features and allows one to obtain the transition energies with four significative digits. Just a few experimental points are displayed in Figure 3 to show better the fit of the theoretical curve. Figure 4 shows the logarithmic plot of the data points in the less steep side of the maximum of Figure 3. Again, the experimental points rapidly go asymptotically to a straight line of -1 slope with high precision.

Figure 5 shows what happens when a small constant is uniformly added to the absorbance data. The data points do not go asymptotically to a straight line with -1 slope and acquire some curvature when the added constant is not very small (not shown in Figure 5). Hence, logarithmic plots such as those of Figures 2, 4, and 5 constitute a good test for the proper choice of the background level in the analysis of the experimental peaks. Background levels linear in the relative energies $\hbar ck - E_{l'l}$ or following more complex functions may be assayed for peaks not completely resolved. A good criterion for choosing the right parameters for the function representing the nonuniform background profile should be given by the logarithmic plot of the presumed net absorbance in the less steep side of the peak, which should go asymptotically to a straight -1 slope line when the parameters are well chosen.

In general, eq 16 fits most near- and far-infrared asymmetric spectral features as well as it does for the two examples shown in this section. In addition to their intrinsic interest, these two cases were chosen from the quite extense literature because they

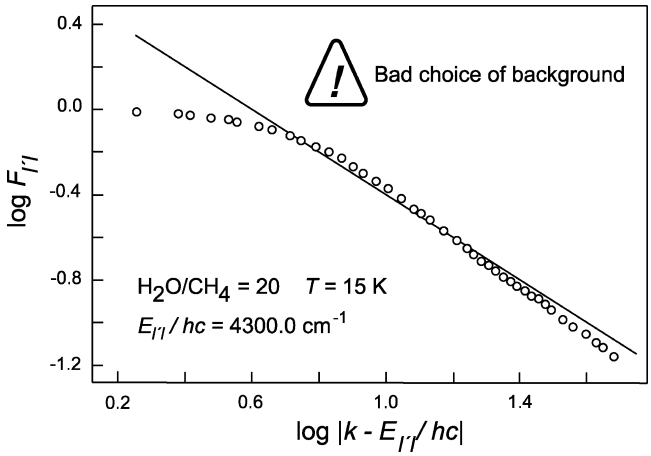

Figure 5. Data of Figures 3 and 4 with a small constant background level added. The so-modified data do not go asymptotically to the straight line with slope −1. This kind of logarithmic plot provides a rapid and objective method for choosing the proper background level.

exhibit the absorption peaks in a particularly thorough manner. We also take care of selecting peaks with fairly different characteristics.

The Asymptotic Character of Equation 16. In the limit of very small electron−phonon coupling coefficients, g_{ql}, the line shape function $F_{l'l}$ should go to a δ-function. Writing eq 5 for $|\vec{q}| \ll 1/a$, where a is a typical lattice spacing, one has

$$g_{ql} = \sqrt{\frac{\hbar}{2NM_{\vec{l}}\omega_q}}\hat{e}_{\mathrm{q}} \cdot \sum_{\vec{l}'} (1 + i\vec{q}\cdot\vec{l}')\vec{F}_{\alpha(\vec{l}-\vec{l}')} \qquad (19)$$

However,

$$\sum_{\vec{l}'} \vec{F}_{\alpha(\vec{l}-\vec{l}')} = 0 \qquad (20)$$

because it is the net mean force excerted on the ion at the lattice site $\vec{l}$. Therefore, the coefficients g_{ql} vanish for $|\vec{q}| = 0$ and are linear in $|\vec{q}|$ for small values of $|\vec{q}|$. Because we are considering just acoustic modes, the frequencies, ω_q, are also linear in $|\vec{q}|$ and vanish for $|\vec{q}| = 0$. With this in mind, from examining eqs 5 and 6,

$$|G_{ql'l}|^2 \propto |\vec{q}|^{-1} \quad \text{for} \quad |\vec{q}| \ll 1/a \qquad (21)$$

Consider now eqs 17 and 18 for $\Gamma_{l'l}$ and $\delta_{l'l}$. Because the density of modes with respect to $|\vec{q}|$ is proportional to $|\vec{q}|^2$, the coefficients multiplying $\delta_1(\omega_q)$ in both equations vanish for $|\vec{q}| = 0$. Therefore,

$$\Gamma_{l'l} = \delta_{l'l} = 0 \qquad \text{if } \delta_1(\omega_q) = \delta(\omega_q) \qquad (22)$$

In other words, both $\Gamma_{l'l}$ and $\delta_{l'l}$ vanish if δ_1 is a true δ-function, and the line shape function $F_{l'l}$ becomes a δ-function centered at $\hbar ck = E_{l'l}$. Therefore, the finite width of the spectral line demands that δ_1 be a finite distribution.

Acknowledgment. This work is supported by the Chile Bicentennial Program in Science and Technology Grant ACT 26, Center for Research and Applications in Plasma Physics and Pulsed Power Technology (P4 Project). F.A.A. thanks to Mecesup Doctoral Fellowship. R.H., D.P., and P.S.M. are grateful to CONICYT for doctoral fellowships.

References and Notes

(1) Rebane, K. K. *Impurity Spectra of Solids*; Plenum Press: New York, 1970.
(2) Stoneham, A. M. *Theory of Defects in Solids*; Clarendon Press: Oxford, 1975.
(3) Fowler, W. B., Ed.; *Physics of Color Centers*; Academic Press: New York & London, 1968.
(4) Osad'ko, I. S. *Selective Spectroscopy of Single Molecules*; Springer: Berlin, 2003.
(5) Takeno, S.; Sievers, A. J. *Phys. Rev. Lett.* **1965**, *15*, 1020–1023.
(6) Lagos, M.; Asenjo, F.; Hauyón, R.; Pastén, D; González, H.; Henríquez, R.; Troncoso, R. *Phys. Rev. B* **2008**, *77*, 104305 (1−10).
(7) Balzar, D. In *Defect and Microstructure Analysis from Diffraction*; Snyder, R. L., Bunge, H. J., Fiala, J., Eds.; International Union of Crystallography Monographs on Crystallography No. 10, Oxford University Press: New York, 1999, pp 94−126.
(8) Stancik, A. L.; Brauns, E. B. *Vib. Spectrosc.* **2008**, *47*, 66–69.
(9) Sild, O; Rebane, K. K. *Opt. Spectrosc.* **2001**, *90*, 686–690.
(10) Sild, O; Haller, K., Eds.; *Zero-Phonon Lines and Spectral Hole Burning in Spectroscopy and Photochemistry*; Springer: Berlin, 1998.
(11) Hizhnyakov, V.; Holmar, S.; Tehver, I. *J. Lumin.* **2007**, *127*, 7–12.
(12) Huang, K.; Rhys, A. *Proc. R. Soc. London, Ser. A* **1950**, *204*, 406–423.
(13) Franck, J. *Trans. Faraday Soc.* **1925**, *21*, 536–542.
(14) Condon, E. U. *Phys. Rev.* **1928**, *32*, 858–872.
(15) Gerakines, P. A.; Bray, J. J.; Davies, A.; Richey, C. R. *Astrophys. J.* **2005**, *620*, 1140–1150.
(16) Bernstein, M. P.; Cruikshank, D. P.; Sanford, S. A. *Icarus* **2006**, *181*, 302–308.

JP103459P